

This discussion paper is/has been under review for the journal Atmospheric Measurement Techniques (AMT). Please refer to the corresponding final paper in AMT if available.

MIAWARA-C, a new ground based water vapor radiometer for measurement campaigns

C. Straub, A. Murk, and N. Kaempfer

Institute of Applied Physics, University of Berne, Berne, Switzerland

Received: 18 May 2010 – Accepted: 21 May 2010 – Published: 28 May 2010

Correspondence to: C. Straub (corinne.straub@iap.unibe.ch)

Published by Copernicus Publications on behalf of the European Geosciences Union.

AMTD

3, 2389–2432, 2010

MIAWARA-C

C. Straub et al.

Title Page

Abstract

Introduction

Conclusions

References

Tables

Figures

⏪

⏩

◀

▶

Back

Close

Full Screen / Esc

Printer-friendly Version

Interactive Discussion



Abstract

In this paper a new 22 GHz water vapor spectro-radiometer which has been specifically designed for profile measurement campaigns of the middle atmosphere is presented. The instrument is of a compact design and has a simple set up procedure. It can be operated as a standalone instrument as it maintains its own weather station and a calibration scheme that does not rely on other instruments or the use of liquid nitrogen. The optical system of MIAWARA-C combines a choked gaussian horn antenna with a parabolic mirror which reduces the size of the instrument in comparison with currently existing radiometers. For the data acquisition a correlation receiver is used together with a digital cross correlating spectrometer. The complete backend section, including the computer, is located in the same housing as the instrument. The receiver section is temperature stabilized to avoid gain fluctuations. Calibration of the instrument is achieved through a balancing scheme with the sky used as the cold load and the tropospheric properties are determined by performing regular tipping curves. Since MIAWARA-C is used in measurement campaigns it is important to be able to determine the elevation pointing in a simple manner as this is a crucial parameter in the calibration process. Here we present two different methods; scanning the sky and the Sun. Finally, we report on the first spectra and retrieved water vapor profiles acquired during the Lapbiat campaign at Sodankylä Geophysical Observatory. The performance of MIAWARA-C is validated here by comparison of the presented profiles against the equivalent profiles from the Microwave Limb Sounder on the EOS/Aura satellite.

1 Introduction

Water vapor is a key element in the Earth's radiative budget as it is the most important greenhouse gas in the upper troposphere and contributes to the radiative cooling of the stratosphere by infrared emission. Alongside this it is also involved in several chemical processes, one of which is ozone depletion, where it acts as the main source

AMTD

3, 2389–2432, 2010

MIAWARA-C

C. Straub et al.

Title Page

Abstract

Introduction

Conclusions

References

Tables

Figures

◀

▶

◀

▶

Back

Close

Full Screen / Esc

Printer-friendly Version

Interactive Discussion



of the reactive OH radical. In the stratosphere water vapor has a long chemical lifetime with respect to the time scale of dynamical processes and can therefore be used as a tracer to investigate phenomena such as stratosphere-troposphere exchange, meridional transport and polar vortex containment.

5 Approximately half of the water vapor in the middle atmosphere enters it by vertical transport through the tropical tropopause where solar irradiation is at its greatest, creating a strong upward stream of air called the “tropical pipe”, which reaches from the troposphere up to the stratosphere (Plumb, 1996). The other main source of middle atmospheric water vapor is the oxidation of methane leading to an increase in the volume mixing ratio with increasing altitude in the stratosphere. Photo-dissociation due to the absorption of solar UV-radiation is the only relevant sink of water vapor in the middle atmosphere, leading to a decrease in the volume mixing ratio with increasing altitude throughout the mesosphere.

10 Water vapor in the upper stratosphere and mesosphere is mainly observed by passive remote sensing instruments, either space borne or ground based. While satellite instruments, such as MLS on EOS/Aura (Waters et al., 2006), MIPAS on ENVISAT (Milz et al., 2005) and ODIN (Murtagh et al., 2002) provide the vertical as well as the horizontal distribution of water vapor, ground based instruments provide vertical profiles in a single location. Ground based instruments are characterized by long operational lifetimes while the lifetime for satellites is typically limited to less than 10 yr. Therefore measurements from the ground are important for long term monitoring of water vapor and the merging of consecutive satellite missions. Thus, long term global datasets can be generated, which are crucial for climate research.

25 For middle atmospheric water vapor profiling from the ground the rotational transition at 22 GHz is typically used since at this frequency the tropospheric opacity is low and therefore this line can be observed even from sea level. There are few ground based spectro-radiometers at 22 GHz operating on a regular basis, e.g. the instruments in Ny-Ålesund (Norway) (refurbishment 2008–2011), Andoya (Norway), Seoul (South Korea) in addition to the NDACC instruments in Onsala (Sweden) (Forkman et al., 2003),

Title Page

Abstract

Introduction

Conclusions

References

Tables

Figures

◀

▶

◀

▶

Back

Close

Full Screen / Esc

Printer-friendly Version

Interactive Discussion



Bern (Switzerland) (Deuber et al., 2004), Table Mountain (California, USA), Mauna Loa (Hawaii, USA) and Lauder (New Zealand) (Thacker et al., 1995), (Nedoluha et al., 1995) and (Nedoluha et al., 2007). There have also been several new developments in recent years, e.g. the instruments on the Zugspitze (Germany), Kuehlungsborn (Germany), Karlsruhe (Germany) and the Mobile Microwave Radiometer operated by the University of Toulouse (France) (Motte et al., 2008).

The instrument we present here is the third 22 GHz microwave radiometer for middle atmospheric water vapor built by the Institute of Applied Physics, University of Bern. The first was the Middle Atmospheric Water vapor Radiometer (MIAWARA) (Deuber et al., 2004) which started routine operation near Bern in 2002 and is part of NDACC since 2005. The second instrument, the Stratospheric Water Vapour Radiometer (SWARA), is a joint project of the University of Bern and the Sookmyung Women's University of Seoul, South Korea and began operation in Seoul in 2006. It was designed as a copy of MIAWARA.

The motivation behind the construction of the new MIAWARA-C instrument presented here was to have a microwave instrument that could be easily transported and would therefore be well suited for use in measurement campaigns. A significant advantage to this design is that it can act as a traveling standard for intercomparisons between the other instruments currently in routine operation, and it can also participate in measurement campaigns as an independent ground based instrument covering an altitude range complementary to the altitudes of other profiling techniques like radiosondes, LIDAR and FTIR. MIAWARA-C, shown in Fig. 1, is a standalone instrument that requires only electrical power and an internet connection since the backend and the computer are included in the housing. The calibration concept is independent of any information from other instruments or liquid nitrogen and the rainhood closes automatically whenever there is precipitation or strong winds to prevent the instrument from damage. The temperature and ground pressure data needed for the calibration comes from a weather station (of type WTX520 from Vaisala) which is attached to the instrument.

MIAWARA-C

C. Straub et al.

Title Page

Abstract

Introduction

Conclusions

References

Tables

Figures

◀

▶

◀

▶

Back

Close

Full Screen / Esc

Printer-friendly Version

Interactive Discussion



MIAWARA-C

C. Straub et al.

[Title Page](#)[Abstract](#)[Introduction](#)[Conclusions](#)[References](#)[Tables](#)[Figures](#)[◀](#)[▶](#)[◀](#)[▶](#)[Back](#)[Close](#)[Full Screen / Esc](#)[Printer-friendly Version](#)[Interactive Discussion](#)

In the second section of this paper we present the instrumental set-up of MIAWARA-C, focusing on the optical system and the correlation receiver. The initial premise was to use this receiver together with an internal cold noise source for a real-time balancing to calibrate the instrument. An introduction to this calibration concept with its advantages and crucial limitations is given in this section. In the third section we present the calibration scheme used for MIAWARA-C, which is a hybrid between internal and external balancing. In the fourth section we describe two different methods for the validation of the instrumental pointing; scanning of the sky and the Sun. The fifth section is dedicated to the first spectra and profiles acquired with MIAWARA-C. We also provide comparisons of the results with those from Aura/MLS.

2 Measurement principle and instrumental set-up

MIAWARA-C measures the spectral intensity of the pressure broadened water vapor emission line at 22.235 GHz. The shape of this line can be related to the vertical distribution of water vapor in the atmosphere because the pressure decreases exponentially with altitude. For MIAWARA-C, a retrieval algorithm based on the optimal estimation technique described in Rodgers (2000), is used to retrieve water vapor profiles from the measured spectra. In the middle atmosphere retrievals are possible at altitudes between approximately 30 and 80 km. The upper limit is given by the frequency resolution of the spectrometer and the Doppler broadening effect while the lower limit is given by the bandwidth of the spectrometer and the distortion of the spectrum by instrumental artifacts, known as the baseline.

In microwave radiometry the intensity of radiation is usually expressed in terms of brightness temperature T_b according to the Rayleigh-Jeans approximation of Plank's law. The brightness temperature of the atmosphere along a certain line of sight observed from the ground is a superposition of emission and absorption of radiation at

MIAWARA-C

C. Straub et al.

[Title Page](#)[Abstract](#)[Introduction](#)[Conclusions](#)[References](#)[Tables](#)[Figures](#)[⏪](#)[⏩](#)[◀](#)[▶](#)[Back](#)[Close](#)[Full Screen / Esc](#)[Printer-friendly Version](#)[Interactive Discussion](#)

the received signal. The antenna beam of MIAWARA-C has a Half Power Beam Width (HPBW) of 5.0° , corresponding to a directivity of 31.7 dB. To keep the antenna as small as possible a horn with a relatively low directivity of 23.8 dB was chosen and combined with a focusing parabolic mirror to achieve the required directivity of 31.7 dB.

The horn antenna used for MIAWARA-C is a choked Gaussian horn (Teniente et al., 2002), whose geometry was optimised to achieve an antenna pattern of high rotational symmetry with sidelobes below -40 dB. During calibration the mirror is slewed, making the high rotational symmetry of the horn antenna beam important. Were the beam in any way asymmetrical the calibration process would lead to a mismatch between the horn and the mirror and thus would introduce systematic errors in beam coupling. The low side lobe level is crucial so as to maintain the required high level of beam efficiency since the signal received from the stratosphere has a line amplitude of only approximately 0.2 K. With higher sidelobe levels the radiometer would intercept power from directions other than from the atmosphere, leading to systematic errors in the antenna temperature.

To keep spillover losses small the parabolic mirror needs to be as large as possible. However, as MIAWARA-C is a campaign instrument that is required to travel, the mirror dimensions must also be kept to a reasonable minimum. Therefore, the size of the mirror is a trade off between those two requirements. The geometry of the mirror was optimized using physical optics simulations to maintain a constant edge taper below -35 dB. This resulted in an elliptical rim with major and minor axes of 39 cm and 27.8 cm, respectively. A 90° off axis geometry was chosen to enable an easy switching of the mirror for the calibration process.

Using the choked Gaussian antenna instead of a conventional conical corrugated horn antenna ensured a greater than threefold reduction in spillover loss for the optimized mirror from 0.21% to 0.06% of the received power. Another advantage to this choice of horn is its relatively short length (approximately 15 cm). This is half the length of an equivalent conical corrugated horn. The choked Gaussian horn thus ensures a reduced mirror diameter and horn length, thus minimising the dimensions of the

overall instrument.

The plots in Fig. 4 show the measured farfield pattern of the optical system of MIAWARA-C at 22.235 GHz. These measurements were performed using two methods. A description of the first method using a laboratory setup with a rectangular horn as transmitter is given in de Wachter et al. (2009). The beam patterns measured using the first method are shown in red (E and H horizontal) and black (E and H zenith). The measurements reveal that the antenna pattern is almost identical for the antenna pointing to the zenith and to the horizon. There exists small asymmetry between the H-plane in the zenith and the E-plane in the horizon which is attributed to the off-axis orientation of the mirror. Since this asymmetry does not lie in the scanning direction of the mirror it does not affect the measurements.

A description of the second method using the Sun as a transmitter is given in Sect. 4. The result of this measurement is a general antenna pattern since the radiation coming from the sun is not polarized. Comparing the two techniques the measurements reveal a high degree of agreement.

2.2 Correlation receiver

For the radiometric observation of weak emission lines in the microwave region balancing is a well known calibration technique (Parrish et al., 1988). The two radiometers previously built by the IAP in Bern; MIAWARA (Deuber et al., 2004) and SWARA, use a balancing scheme with an external reference load. The initial intention for MIAWARA-C was for it to be used as a correlation receiver together with an internal cold calibration load, known as a Colfet, to balance the sky brightness temperature. A receiver of this type significantly reduces integration time as it does not need to be calibrated as frequently as a conventional balancing receiver thanks to a high system stability (cf. Fig. 5). It is not necessary to direct the mirror to an additional reference load as the balancing occurs internally in real time. Unfortunately, due to linearity problems of the spectrometer and the significantly high temperature of the Colfet additional external balancing is needed to obtain a spectrum without significant baseline artifacts

Title Page

Abstract

Introduction

Conclusions

References

Tables

Figures



Back

Close

Full Screen / Esc

Printer-friendly Version

Interactive Discussion



and the correlation receiver is now used as a hybrid between the two calibration techniques. This section gives an overview of the correlation receiver of MIAWARA-C and a short introduction to the initial calibration concept with its advantages and limitations. A detailed description of the calibration concept actually used can be found in the next section.

2.3 The receiver

The correlation receiver of MIAWARA-C, schematically shown in Fig. 2, consists of two identical heterodyne receivers connected by a hybrid coupler. There are two RF signals, one from the horn antenna and the other from a Colfet noise source (equivalent temperature ~ 140 K) entering the receiver. The two RF signals are split equally between the two identical radiometer chains by the 90° hybrid coupler. In the receivers the noise signals are amplified, band limited and down converted to the frequency range of the spectrometer.

The digital Correlation and Spectrum Analysis backend (CoSpAn) was realized in an Acqiris AC 240 board having two input channels and a fast Field Programmable Gate Array (FPGA).

The original FFT firmware for this spectrometer allowed for the calculation of the power spectrum from time domain signals in real-time for one of the input channels. Descriptions of this concept can be found in (Müller et al., 2006) and (Benz et al., 2005).

For CoSpAn the FFT software has been customized to calculate a complex cross-correlation between the signals on the two input channels. In the FPGA core of the correlator each of the incoming signals is fast Fourier transformed separately and a complex multiplication is calculated. CoSpAn has a bandwidth of 500 MHz and 2^{14} channels, which corresponds to a frequency resolution of 30.5 kHz.

CoSpAn also allows for operation of the spectrometer in FFT mode with the same bandwidth and resolution simultaneously for both inputs of the spectrometer.

A detailed mathematical description of the correlation receiver of MIAWARA-C can

Title Page

Abstract

Introduction

Conclusions

References

Tables

Figures

⏪

⏩

◀

▶

Back

Close

Full Screen / Esc

Printer-friendly Version

Interactive Discussion



be found in Straub (2008). The output detected is proportional to the difference between the antenna temperature T_a and the brightness temperature of the Colfet $T_{b,\text{colfet}}$:

$$C(v) = a(v) \left(\frac{T_{b,\text{colfet}}(v) - T_a(v)}{2} \right) \quad (3)$$

Here a is a calibration constant proportional to the product of the gains of the two receivers, which makes the receiver less sensitive to gain drifts than a total power receiver. In Fig. 5 the results of stability tests for the receiver operated in the CoSpAn as correlation receiver as well as in the FFT mode as total power receiver are shown. For the purpose of testing the antenna was pointed to an ambient temperature absorber, which here acts as the hot calibration target, and data was sampled in 2 s intervals. The frequency mean of the data was calibrated to brightness temperature of the absorber to give an indication of the temperature fluctuations in degrees Kelvin, as displayed in the leftmost plot in Fig. 5. The Allan variance of the same datasets is shown in the plot on the right. Both representations of the stability of the receivers show that the correlation receiver is less affected by gain fluctuations than the total power receiver.

2.3.1 Initial calibration scheme

The initial concept for calibration of the instrument was to use the correlation receiver together with the Colfet to achieve an internal balancing. Assuming that the brightness temperature of the Colfet $T_{b,\text{colfet}}$ is known the detected line signal can be calibrated with the following formula:

$$T_{b,\text{line}} = T_{b,\text{colfet}} - \frac{C_{\text{line}}}{C_{\text{hot}}} (T_{b,\text{colfet}} - T_{\text{hot}}) \quad (4)$$

where C_{hot} is the measurement of the brightness temperature a of calibration target at ambient temperature T_{hot} . This calibration method has the advantage that only one calibration measurement is necessary to determine the sky brightness temperature. How often the receiver needs to be calibrated depends on the stability of the system.

Title Page

Abstract

Introduction

Conclusions

References

Tables

Figures

⏪

⏩

◀

▶

Back

Close

Full Screen / Esc

Printer-friendly Version

Interactive Discussion



[Title Page](#)[Abstract](#)[Introduction](#)[Conclusions](#)[References](#)[Tables](#)[Figures](#)[⏪](#)[⏩](#)[◀](#)[▶](#)[Back](#)[Close](#)[Full Screen / Esc](#)[Printer-friendly Version](#)[Interactive Discussion](#)

In this instance the system stability is high and thus over 50% of the operating time can be devoted to actual measurement. As mentioned previously the brightness temperature of the Colfet is approximately 140 K, which is too high to correctly balance the sky brightness temperature at 22 GHz, which for an elevation angle of 25° is between 10 and 20 K. It was not possible to locate a noise source of suitably low brightness temperature for the stated requirements. Nevertheless, calibration would be possible if the receiver and the spectrometer were ideal.

In Fig. 6 the plot on the left displays a spectrum calibrated with the method above. There are several artifacts visible. Firstly there are spikes affecting single channels that can easily be removed. Secondly there is a slope originating from standing waves within the system and a possible frequency dependence of $T_{b, \text{colfet}}$ which can likely be removed through fitting a superposition of sine waves to the spectrum. The third and strongest type of artifact are those that originate from nonlinearities of the spectrometer. One such artifact is visible as a wide change in amplitude at frequencies between 22.17 and 22.21 GHz and is marked with a red circle. A sufficiently accurate method of controlling these spectral nonlinearities could not be determined and as such additional external balancing is needed to calibrate the output of MIAWARA-C.

3 Balancing observation

The calibration of MIAWARA-C is divided into two parts. Each cycle starts with a tipping curve to determine the tropospheric opacity and to have a measurement of the hot load and the cold sky calibration target. Following this the beam is continuously switched between the sky and the reference load for the balancing calibration. On average the calibration cycle takes 15 min, of which approximately 38% is devoted to the line measurement.

The process of external balancing involves measuring a reference signal C_{ref} that has the same intensity as the line measurement C_{line} , but which has little or no contribution from the water vapor line at 22 GHz. The difference between the two measurements

is used to calculate the balanced sky brightness temperature ΔT_b . This is illustrated in the right-most plot of Fig. 6 which is itself an ideal representation of the spectrum of the water vapor line and is given by the following equation:

$$\Delta T_b = T_{b,\text{line}} - T_{b,\text{ref}} = \frac{C_{\text{line}} - C_{\text{ref}}}{C_{\text{hot}} - C_{\text{cold sky}}} (T_{\text{hot}} - T_{b,\text{cold sky}}); \quad (5)$$

5 where $T_{b,\text{line}}$ is the sky brightness temperature in the direction of the line measurement and $T_{b,\text{ref}}$ is the temperature in the direction of the reference measurement. For the absolute calibration there are two targets; a microwave absorber that is used as hot load, and the sky under an elevation angle of 65° which represents the cold load. The sky brightness temperature at a certain elevation angle can be approximated by using
 10 a simplified version of the RTE, Eq. (1), assuming the troposphere as a single layer with a mean temperature T_{eff} :

$$T_b^{\text{sky}}(\theta) = T_0 e^{-A_\theta^{\text{trop}} \tau_z} + T_{\text{eff}} (1 - e^{-A_\theta^{\text{trop}} \tau_z}) \quad (6)$$

where τ_z is the opacity in zenith direction and A_θ is the airmass factor at the elevation angle θ . This approach is used to find the brightness temperature of the sky used as
 15 the cold load. The determination of the tropospheric opacity is described in the next section. Trigonometrical considerations lead to the following formula for the airmass factors of the troposphere and middle atmosphere (will be used later):

$$A^{\text{trop}} = \frac{\sqrt{(R+z)^2 - R^2 \cos^2 \theta} - R \sin \theta}{z} \quad (7)$$

and

$$20 \quad A^{\text{ma}} = \frac{\sqrt{(R+z+H)^2 - R^2 \cos^2 \theta} - \sqrt{(R+z)^2 - R^2 \cos^2 \theta}}{H} \quad (8)$$

where R is Earth's radius, z is the height of the tropopause and H is the height of the middle atmosphere from tropopause to mesopause.

Title Page

Abstract

Introduction

Conclusions

References

Tables

Figures

◀

▶

◀

▶

Back

Close

Full Screen / Esc

Printer-friendly Version

Interactive Discussion



The mean tropospheric temperature T_{eff} can be estimated using the ambient temperature on the ground T_{amb} :

$$T_{\text{eff}} = c_1(T_{\text{amb}} - 273.15) + c_0 \quad (9)$$

where the values of the coefficients c_1 and c_0 are those derived experimentally by (Han and Westwater, 2000); namely $c_1=0.69$ and $c_0=266.3$.

The elevation angle for the line observation is chosen to achieve a maximum signal to noise ratio. The intensity of the observed water vapor signal depends on the path length through the middle atmosphere. This implies that the lower the elevation angle at which the line is observed, the longer the path length which leads to a stronger signal. Conversely, a lower elevation angle implies a stronger attenuation in the troposphere. Results from (Haefele, 2009) show that for tropospheric opacities below 0.2 the signal to noise ratio increases for decreasing elevation angles down to approximately 15° , beyond which it decreases further. Therefore for line observation elevation angles between 15° and 25° are required.

For the reference measurement the antenna of MIAWARA-C is directed to the zenith where the path length is a minimum. Microwave absorber is inserted into the beam which ensures that the measured intensity equals the emission of the sky at the elevation angle of the observation. During the balancing measurement the antenna beam is repeatedly switched between the fixed reference and adjusted line measurement in such a way that the elevation of the line measurement is manipulated in order to minimize $C_{\text{line}} - C_{\text{ref}}$.

The brightness temperature as measured in what is referred to as the “line direction”, $T_{\text{b,line}}$, from the ground can be divided into the microwave background radiation T_0 plus the water vapor emission line originating in the middle atmosphere $T_{\text{b,z}}^{\text{ma}}$, scaled with the airmass factor for the line measurement, and the continuum emission in the troposphere approximated as mean tropospheric temperature T_{eff} . For the part of the radiation originating above the tropopause, namely T_0 and $T_{\text{b,z}}^{\text{ma}}$, one needs to consider

Title Page

Abstract

Introduction

Conclusions

References

Tables

Figures

⏪

⏩

◀

▶

Back

Close

Full Screen / Esc

Printer-friendly Version

Interactive Discussion



the attenuation in the troposphere:

$$T_{b,\text{line}} = (T_{b,z}^{\text{ma}} A_{\text{line}}^{\text{ma}} + T_0) e^{-A_{\text{line}}^{\text{trop}} \tau_z} + T_{\text{eff}} (1 - e^{-A_{\text{line}}^{\text{trop}} \tau_z}) \quad (10)$$

Here A is the airmass factor of the specified atmospheric layer (ma=middle atmosphere, trop=troposphere) for the specified measurement and τ_z is the tropospheric opacity in the zenith direction.

The same separation between radiation originating above and below the tropopause can be made when regarding the sky brightness temperature in the reference direction. However, the influence of the microwave absorber in the beam needs to be taken into account:

$$T_{b,\text{ref}} = T_{b,\text{ref}}^* t + (1 - t) T_{\text{abs}} \quad (11)$$

with

$$T_{b,\text{ref}}^* = (T_{b,z}^{\text{ma}} A_{\text{ref}}^{\text{ma}} + T_0) e^{-A_{\text{ref}}^{\text{trop}} \tau_z} + T_{\text{eff}} (1 - e^{-A_{\text{ref}}^{\text{trop}} \tau_z}) \quad (12)$$

where T_{abs} is the physical temperature of the reference absorber and $T_{b,\text{ref}}^*$ the brightness temperature of the sky in the reference direction. The contribution of the absorber bar to the reference signal is regarded in terms of an equivalent transmission, t , of the reference absorber. This equivalent transmission of the reference bar indirectly depends on the opacity of the troposphere and is therefore not constant and needs to be determined for each measurement. The line signal from the middle atmosphere is present in the measurement in the reference direction. This is taken into account when the balanced spectrum is corrected for the attenuation in the troposphere, as will be discussed in Sect. 5.

3.1 Tropospheric opacity

To estimate the tropospheric opacity the iterative approach described in Han and Westwater (2000) is used. The basic premise of this method is to measure the sky at two or

Title Page

Abstract

Introduction

Conclusions

References

Tables

Figures

⏪

⏩

◀

▶

Back

Close

Full Screen / Esc

Printer-friendly Version

Interactive Discussion



more different elevation angles and to relate the spectrometer outputs to sky brightness temperatures using the RTE (Eq. 1). For the tipping calibration of MIAWARA-C seven different angles in an elevation range between 25° and 50° are measured.

The opacity is then found by iteration of the following four steps:

1. The brightness temperature of the cold-sky calibration target $T_{b,cold\ sky}$ is calculated using the RTE for the Troposphere (Eq. 6). For the first iteration an initial estimated value of 0.3 is used for the zenith opacity.

2. The measurements at the tipping elevations are calibrated using hot-cold calibration,

$$T_{b,\theta} = \frac{C_{\theta} - C_{hot}}{C_{hot} - C_{cold\ sky}} (T_{hot} - T_{b,cold\ sky}) + T_{hot}; \quad (13)$$

where $T_{b,\theta}$ is the microwave brightness temperature at the elevation angle θ , C_x are the measured spectrometer outputs at the various targets and T_{hot} is the physical temperature of the hot calibration target. The brightness temperature of the cold sky $T_{b,cold\ sky}$ is determined using Eq. (6).

3. The opacity at the tipping angles is calculated from the calibrated measurements using the following relation:

$$\tau_{\theta} = \ln \left(\frac{T_{eff} - T_0}{T_{eff} - T_{b,\theta}} \right) \quad (14)$$

4. The zenith opacity τ_z is given by the slope of a linear fit of τ_{θ} versus the airmass A , since in zenith direction $A=1$.

The linear fit must go through the origin of the coordinate system, since the opacity must be zero if there is no atmosphere. The iteration is stopped when the offset of the fit lies below 10^{-3} . In practice the process presented here typically converges after the second iteration.

Title Page

Abstract

Introduction

Conclusions

References

Tables

Figures

◀

▶

◀

▶

Back

Close

Full Screen / Esc

Printer-friendly Version

Interactive Discussion



3.1.1 Validation of tipping-curve calibration

To validate the opacities found with the tipping curve calibration a time series of tropospheric zenith opacity mean values obtained during one and a half months in the Summer of 2009 in Bern are compared to those obtained using the TROWARA microwave radiometer which observed from the same location as MIAWARA-C but for a slightly different pointing (MIAWARA-C: south, TROWARA: south-east).

TROWARA monitors the sky brightness temperature at a constant elevation angle of 40° in three frequency bands at 21.3, 22.2 and 31.5 GHz, (Mätzler and Morland, 2009). For this comparison only the channel at 22.2 ± 0.2 GHz is used.

The results of this comparison are displayed in Fig. 7 as a time series plot (left) and a scatter plot (right). TROWARA measures the sky brightness temperature at one second intervals while MIAWARA-C performs a tipping curve to determine the tropospheric opacity every 15 min. Four hourly means of the two datasets are used to suppress the measurement noise and to reveal any possible systematic bias. The mean difference between the opacities determined with the two instruments is 0.1% with a standard deviation of 5.7%, where the values obtained with MIAWARA-C are slightly higher than those from TROWARA. The correlation coefficient r is 0.97.

One possible explanation for the values obtained with MIAWARA-C being slightly higher than those from TROWARA is that the bandwidth of the data used for the determination of the opacity was 200 MHz for MIAWARA-C and 400 MHz for TROWARA. Since the positive slope in the opacity decreases with increasing frequency the mean value is expected to be higher for the smaller bandwidth.

3.1.2 Validation of the temperature of $T_{\text{cold sky}}$

The temperature of the cold sky determined by the tipping curve calibration is validated using liquid nitrogen calibration. For a comparison of the cold sky temperatures liquid nitrogen and tipping curve measurements are performed alternately. Three measurements, each lasting approximately three hours were performed on three different days

Title Page

Abstract

Introduction

Conclusions

References

Tables

Figures

⏪

⏩

◀

▶

Back

Close

Full Screen / Esc

Printer-friendly Version

Interactive Discussion



during the Summer of 2009 in Bern. From these measurements the difference in the brightness temperature of the cold sky, $\Delta T_{\text{cold sky}}$, determined using the two different methods is found. The mean value of the difference is 0.7 K (1.8% of the mean temperature of the cold sky) with a standard deviation of 1.9 K (5.2% of the mean temperature of the cold sky). It was found that due to reflexions on the air liquid nitrogen interface the microwave brightness temperature of liquid nitrogen was difficult to determine and thus it was concluded that the tipping curve calibration of $T_{\text{cold sky}}$ was of good quality. This result also shows that there is no obstacle in the beam at ambient temperature (e.g. the reference absorber) affecting measurement in cold sky direction.

4 Validation of instrumental pointing

An offset in the elevation pointing would lead to a systematic error in the sky brightness temperatures. Therefore, it is crucial that the elevation angle is determined with the highest possible accuracy. For MIAWARA-C the elevation pointing needs to be determined for every campaign after setting up the instrument. The two different methods used are scanning the sky and the Sun. The sky scanning requires an unobstructed view from between approximately 60° to 120° elevation while for the Sun scanning the Sun needs to pass through the field of view of the instrument at an elevation angle greater than 20° . The appropriate method thus depends on the field of view of the instrument and the solar elevation angle. In the following section results from the Summer 2009 measurement campaign at Bern are presented. Spectral mean values are used for all the calculations.

4.1 Sun-scanning

The ephemerids of the Sun are well known and therefore the sun can be used to determine the pointing of a radiometer in elevation as well as in azimuth, by scanning a certain range (depending on the HPBW of the antenna) around the elevation of the

Title Page

Abstract

Introduction

Conclusions

References

Tables

Figures

◀

▶

◀

▶

Back

Close

Full Screen / Esc

Printer-friendly Version

Interactive Discussion



Sun passing through the antenna beam.

Tropospheric properties must be taken into account when observing the Sun from the ground and therefore a tipping curve calibration is performed for every Sun scanning cycle from which the tropospheric opacity is determined. The expected sky brightness temperature at a certain elevation angle $T_{b,\theta}^{\text{exp}}$ is calculated using the RTE for the Troposphere. The actual sky brightness temperature $T_{b,\theta}^{\text{act}}$ can be determined from a hot-cold calibration where the cold sky observation is performed at an elevation angle that is far away from the Sun (e.g. if for a Sun elevation angle of 30° an acceptable cold sky observation angle would be at approximately 60°). When the Sun passes the antenna beam, the actual sky brightness temperature deviates significantly from the expected one, since it is a linear combination of the brightness temperatures of the Sun and of the atmosphere. Taking the difference between $T^{h-c}(\theta)$ and $T^{\text{RTE}}(\theta)$ results in the convolution of the brightness temperature of the sun and the antenna pattern of the radiometer.

As the sun has an extent of approximately 0.5° on the sky as observed from Earth the sun scanning method may also be used to determine the shape of the antenna pattern (cf. Figs. 8 and 4).

To determine the pointing of the instrument the measurements are transformed to a rectangular coordinate system, shown in Fig. 8 on the left, and a weighted mean value of the antenna pattern is taken in both the azimuth and elevation directions. A Gaussian curve is then fitted to the data, as shown in Fig. 8 on the right. The best fit in the elevation direction is equal to the difference in the actual elevation angle of the instrument and the elevation angle assumed by the instrument's operating software. The best fit for the azimuth direction reveals a deviation in the azimuth pointing in the south. The azimuth pointing is used to determine the location of the actual measurement. The results of a Sun scan performed during the Summer 2009 campaign are shown in Table 2.

Title Page

Abstract

Introduction

Conclusions

References

Tables

Figures

⏪

⏩

◀

▶

Back

Close

Full Screen / Esc

Printer-friendly Version

Interactive Discussion



4.2 Sky scanning

For the sky scanning method the reference bar is removed in order to have an unobstructed view towards the zenith and approximately 20 measurements of the sky for 41 elevation points between 60° and 120° and of the hot calibration target are performed. The sky at an elevation angle of 90° is used as the cold calibration target. Its brightness temperature is determined using the RTE, where the opacity is found with a tipping curve calibration using the measurements at elevation angles between 60° and 89°. The brightness temperature at the sky scanning angles $T_{b,\theta}$ are calculated using hot-cold calibration. Calibrated sky scans performed during the Summer 2009 campaign are shown in Fig. 9 on top.

The zenith direction is where the temperature is the coldest. To find the minimum of the mean value of the calibrated measurements the first derivative is determined, whereupon a third degree polynomial is fitted to the derivative and zeros are searched for. The results of the fitting and the zero-search are shown in Fig. 9 bottom and in Table 2. The same table shows that the sky and Sun scanning methods lead to similar results for the pointing in elevation. From these results it is concluded that the MIAWARA-C pointing accuracy is better than 0.05°.

5 First campaigns and results

The first radiometric measurements from MIAWARA-C were performed at the end of 2008 in Bern, Switzerland (47.0° N, 7.5° E, 550 m) after which it was shipped to the Zugspitze, Germany (47.4° N, 11.0° E, 2650 m) in the beginning of January 2009 for the ARIS Campaign where it remained until the end of April of the same year. In Summer 2009 some minor alterations to the instrument housing were performed (the power supplies were transferred to a new compartement outside of the temperature stabilized part of the housing), upon which it was shipped to the Table Mountain Facility, USA (34.4° N, 117.7° W, 2285 m) in the beginning of September for the MOHAVE 2009

Title Page

Abstract

Introduction

Conclusions

References

Tables

Figures

⏪

⏩

◀

▶

Back

Close

Full Screen / Esc

Printer-friendly Version

Interactive Discussion



campaign. From January to June 2010 MIAWARA-C was operated at the Sodankylä Geophysical Observatory, Finland (67.4° N, 26.6° E, 180 m) where it participated in the Lapbiat campaign. The Lapbiat campaign has to date been the longest and most successful measurement campaign in terms of the amount of data and therefore the data acquired during this time is used here for a first validation of MIAWARA-C against EOS/MLS.

The spectrum relevant for the retrieval of water vapor profiles from MIAWARA-C is at the tropopause level in the zenith direction. The reason to use zenith direction for the retrieval is that for the line observation the elevation angle is not constant but is continuously adjusted to balance the reference load as the opacity of the troposphere is constantly changing. The tropopause level is chosen so that the information from the troposphere will be suppressed by the balancing technique. In order to determine such a spectrum that is independent of the tropospheric conditions $\Delta T_{b,z}^*$ each balanced spectrum ΔT_b is corrected for the tropospheric attenuation:

$$\Delta T_{b,z}^* = \frac{\Delta T_b}{A_{\text{line}}^{\text{ma}} e^{-A_{\text{line}}^{\text{trop}} \tau_z} - t A_{\text{ref}}^{\text{ma}} e^{-A_{\text{ref}}^{\text{trop}} \tau_z}} - T_{b,\text{res}} \quad (15)$$

where according to Eq. (5) $\Delta T_b = T_{b,\text{line}} - T_{b,\text{ref}}$ results by taking the difference of Eqs. (10) and (11), taking into account that the spectra are balanced. This correction also takes into account that the line signal from the middle atmosphere is not only present in the line- but also in the reference measurement.

The equivalent transmission of the reference absorber t is determined by solving Eq. (11):

$$t = \frac{T_{b,\text{ref}} - T_{\text{abs}}}{T_{b,\text{ref}}^* - T_{\text{abs}}} \quad (16)$$

where the total brightness temperature $T_{b,\text{ref}}$ is found using hot-cold calibration from Eq. (13) and the sky brightness temperature in the reference direction $T_{b,\text{ref}}^*$ using the RTE for the troposphere from Eq. (6).

Title Page

Abstract

Introduction

Conclusions

References

Tables

Figures

◀

▶

◀

▶

Back

Close

Full Screen / Esc

Printer-friendly Version

Interactive Discussion



[Title Page](#)[Abstract](#)[Introduction](#)[Conclusions](#)[References](#)[Tables](#)[Figures](#)[◀](#)[▶](#)[◀](#)[▶](#)[Back](#)[Close](#)[Full Screen / Esc](#)[Printer-friendly Version](#)[Interactive Discussion](#)

$T_{b,res}$ is a frequency dependent residuum term originating from the difference in the tropospheric emission in the line and the reference signal. The instrumental artifacts, known as the baseline, that originate from either the standing wave effects inherent to the receiver system or the frequency dependencies of the antenna pattern are also included in this term, which is dealt with during the retrieval process.

In order to obtain a signal-to-noise ratio from which a sufficiently accurate water vapor profile can be retrieved from the spectrum measured by MIAWARA-C, integrations of measurement times spanning from several hours up to days must be performed. The plot displayed in Fig. 10 shows a typical one day balanced spectrum after the tropospheric correction has been applied. The difference in the noise level in the center and on the wings of the spectrum results from different binning, where there is no binning at the center and a binning of ten channels on the wings. For the profile retrieval the ARTS and QPack software packages, described in (Buehler et al., 2005) and (Eriksson et al., 2005), are used. ARTS is a modular program simulating atmospheric radiative transfer that can be used as a forward operator for the inverse model package Qpack. Qpack uses the optimal estimation model, described in (Rodgers, 2000), for the retrieval process.

Figure 11 on the left shows the profile retrieved from a spectrum with 250 MHz bandwidth around the line center of the one day spectrum shown in Fig. 10. The error bars plotted give an upper limit for the sum of the systematic and the random error. The date of the presented profile was chosen near to a close overpass of the Microwave Limb Sounder MLS on the EOS Aura satellite (Lambert et al., 2007). For the retrieval of the MIAWARA-C H₂O profiles shown here the temperature profile measured by MLS is used for the pressure-Temperature-altitude (pTz) information, the line parameters are taken from JPL 1985 catalog (Poynter and Pickett, 1985) and the broadening parameters from (Liebe, 1989). The MLS climatology with a covariance linearly increasing from 10% at 0.681 hPa to 55% at 0.005 hPa is used as H₂O apriori. The correlation of the apriori covariance is assumed to follow a Gaussian shape.

The plot in the center of Fig. 11 shows a comparison between the profile of MLS

MIAWARA-C

C. Straub et al.

[Title Page](#)[Abstract](#)[Introduction](#)[Conclusions](#)[References](#)[Tables](#)[Figures](#)[◀](#)[▶](#)[◀](#)[▶](#)[Back](#)[Close](#)[Full Screen / Esc](#)[Printer-friendly Version](#)[Interactive Discussion](#)

(red dash-dotted) and the one day profile of MIAWARA-C (blue solid). To achieve an identical vertical resolution between the two profiles the MLS profile was convolved with the averaging kernels and the a priori profile of MIAWARA-C (red solid). From these results it is concluded that the two profiles exhibit overall good agreement. The averaging kernels (AVK) plotted on the right in Fig. 11 show that the single day retrieval of MIAWARA-C can be trusted for altitudes between approximately 6 and 0.05 hPa, where the upper limit can be shifted higher by decreasing the measurement noise with longer integration times. The black dashed line shows the full width at half maximum (FWHM) of the AVK giving an indication of the altitude resolution of the retrieved profile.

The Qpack software package provides a tool for the error analysis of the retrieved data based on the calculation of perturbations for different forward model parameters. An estimation of the uncertainty of the relevant forward model parameters of MIAWARA-C is given in Table 3. These estimated values are based on those determined for MIAWARA given in Haefele (2009). It is desirable to provide an upper limit to the errors and thus a conservative calibration error value of 7% of the tropospheric correction factor is chosen. In Fig. 12 a plot of the vertically resolved estimated $2\text{-}\sigma$ errors of the retrieved profiles is shown. The errors result from different families of uncertainty, namely measurement noise, calibration including pointing, spectroscopy, the temperature profile and the smoothing of the retrieval. The smoothing error can be ignored in the instance where the “true” state of the atmosphere is convolved with the AVK when it is compared to the retrieved profile of MIAWARA-C. The differentiation between random and systematic error is challenging. Here all of the error sources except for the measurement noise and the smoothing error are considered as systematic even if the calibration and temperature errors are random to some extent. Therefore an approximate 16% systematic error for all altitudes is considered the upper limit while the measurement noise marks the lower limit for the random error.

The plots in Figs. 13 and 14 display comparisons between H_2O profiles of MLS and 1-day MIAWARA-C retrievals acquired during the Lapbiat 2010 Campaign. The comparison period is from 15 January to 22 April. The criterion for a collocation of

a MLS profile with the measurement site is $\pm 1^\circ$ (± 110 km) in latitude and $\pm 5^\circ$ (± 460 km) in longitude and results in 83 collocations for the 98 d comparison period. For both comparisons presented the profiles of MLS have been interpolated to the pressure grid of MIAWARA-C.

5 A time series of H₂O volume mixing ratio as observed by the two instruments at six pressure ranges between 10 and 0.03 hPa is shown in Fig. 13 and the relative difference between each profile of MIAWARA-C and the MLS profile closest in time is presented in Fig. 14. The agreement between the measurements of MLS and MIAWARA-C is within 5% for pressure altitudes between 6 and 0.05 hPa. The time evolution in H₂O is similar for the measurements of both instruments at all altitudes.

6 Conclusions

MIAWARA-C is a new ground based radiometer for middle atmospheric water vapor, that combines a very compact optical system with a new type of correlation receiver using a digital high resolution spectrometer. The compact design and easy handling of the instrument make it well suited for use in measurement campaigns, as has already been shown for the ARIS, MOHAVE 2009 and Lapbiat campaigns.

15 Tipping curve measurements are used to determine the tropospheric opacity which is used to calculate the temperature of the cold calibration target, namely the sky under an elevation angle of 65° , and to correct the stratospheric signal for attenuation in the troposphere. The tropospheric opacities determined with MIAWARA-C are within 1% of those found with the tropospheric microwave radiometer TROWARA. Liquid nitrogen calibration was used to validate the cold-sky temperature and results showed it to be accurate to within 1 K. This validation was repeated in the beginning of each campaign and every time the reference absorber is changed to assure there is no contamination from the reference bar in the antenna beam while measuring the cold sky calibration target.

25 For the validation of the elevation pointing a Sun and/or the sky scanning method

Title Page

Abstract

Introduction

Conclusions

References

Tables

Figures

⏪

⏩

◀

▶

Back

Close

Full Screen / Esc

Printer-friendly Version

Interactive Discussion



was used, the choice of which was dependent on the location of the instrument. Measurements with both methods at the same location showed that the two techniques provide similar results.

The example of a one day spectrum and retrieval during the Lapbiat campaign show that MIAWARA-C measures spectra with no severe baseline artifacts. A first validation comparing 98 d of MIAWARA-C data to the profiles of MLS indicates that the mean difference between the profiles is below 5% at altitudes between 6 and 0.05 hPa, which is the pressure range for the retrieved profiles from MIAWARA-C that contains the greatest amount of information on the measured spectra. A comparison between time series at different pressure ranges shows that MIAWARA-C and MLS measure similar time evolutions of water vapor volum mixing ratio. The evaluation of the data acquired during the ARIS and the MOHAVE 2009 campaigns will allow for future comparisons of MIAWARA-C profiles with several other instruments.

Acknowledgements. This work has been supported by the Swiss National Science Foundation grant number 200020-124387.

Participation at the Lapbiat campaign was funded through the EU Sixth Framework Programme, Lapland Atmosphere-Biosphere Facility (LAPBIAT2). We thank the team of the Finnish Weather Service for their hospitality and support during the campaign.

Particularly we like to thank the Bern University Reserach Foundation for funding the weather station of MIAWARA-C.

References

- Benz, A. O., Grigis, P. C., Hungerbühler, V., Meyer, H., Monstein, C., Stuber, B., and Zardet, D.: A broadband FFT spectrometer for radio and millimeter astronomy, *Astron. Astrophys.*, 442, 767–773, 2005. 2397
- Buehler, S. A., Eriksson, P., Kuhn, T., von Engeln, A., and Verdes, C.: ARTS, the atmospheric radiative transfer simulator, *J. Quant. Spectrosc. Ra.*, 91, 65–93, 2005. 2409

MIAWARA-C

C. Straub et al.

Title Page

Abstract

Introduction

Conclusions

References

Tables

Figures

◀

▶

◀

▶

Back

Close

Full Screen / Esc

Printer-friendly Version

Interactive Discussion



[Title Page](#)[Abstract](#)[Introduction](#)[Conclusions](#)[References](#)[Tables](#)[Figures](#)[◀](#)[▶](#)[◀](#)[▶](#)[Back](#)[Close](#)[Full Screen / Esc](#)[Printer-friendly Version](#)[Interactive Discussion](#)

- de Wachter, E., Murk, A., Straub, C., Haefele, A., Ka, S., Oh, J. J., and Kämpfer, N.: Effects of resonances in corrugated horn antennas for a 22 GHz balancing radiometer, *IEEE Geosci. Remote*, 6, 3–7, 2009. 2396
- Deuber, B., Kämpfer, N., and Feist, D.: A new 22-GHz radiometer for middle atmospheric water vapor profile measurements, *IEEE T. Geosci. Remote*, 42, 974–984, 2004. 2392, 2396
- Eriksson, P., Jiménez, C., and Buehler, S. A.: Qpack, a general tool for instrument simulation and retrieval work, *J. Quant. Spectrosc. Ra.*, 91, 47–64, 2005. 2409
- Forkman, P., Eriksson, P., and Winnberg, A.: The 22 GHz radio-aeronomy receiver at Onsala Space Observatory, *J. Quant. Spectrosc. Ra.*, 77, 23–42, 2003. 2391
- Haefele, A.: Measurements of Tropospheric, Stratospheric and Mesospheric Water Vapor by Ground Based Microwave Spectro-Radiometry, Ph.D. thesis, University of Bern, 2009. 2401, 2410
- Han, Y. and Westwater, E. R.: Analysis and improvement of tipping calibration for ground-based microwave radiometers, *IEEE T. Geosci. Remote*, 38, 1260–1276, 2000. 2401, 2402
- Lambert, A., Read, W. G., Livesey, N. J., Santee, M. L., Manney, G. L., Froidevaux, L., Wu, D. L., Schwartz, M. J., Pumphrey, H. C., Jimenez, C., Nedoluha, G. E., Cofield, R. E., Cuddy, D. T., Daffer, W. H., Drouin, B. J., Fuller, R. A., Jarnot, R. F., Knosp, B. W., Pickett, H. M., Perun, V. S., Snyder, W. V., Stek, P. C., Thurstans, R. P., Wagner, P. A., Waters, J. W., Jucks, K. W., Toon, G. C., Stachnik, R. A., Bernath, P. F., Boone, C. D., Walker, K. A., Urban, J., Murtagh, D., Elkins, J. W., and Atlas, E.: Validation of the Aura Microwave Limb Sounder middle atmosphere water vapor and nitrous oxide measurements, *J. Geophys. Res.*, 112, D24S36, doi:10.1029/2007JD008724, 2007. 2409
- Liebe, H. J.: MPM – An atmospheric millimeter-wave propagation model, *Int. J. Infrared Milli.*, 10, 631–650, 1989. 2409
- Mätzler, C. and Morland, J.: Refined physical retrieval of integrated water vapor and cloud liquid for microwave radiometer data, *IEEE T. Geosci. Remote*, 47, 1585–1594, 2009. 2404
- Milz, M., von Clarmann, T., Fischer, H., Glatthor, N., Grabowski, U., Höpfner, M., Kellmann, S., Kiefer, M., Linden, A., Tsidu, G. M., Steck, T., Stiller, G. P., Funke, B., López-Puertas, M., and Koukoulis, M. E.: Water vapor distributions measured with the Michelson Interferometer for Passive Atmospheric Sounding on board Envisat (MIPAS/Envisat), *J. Geophys. Res.*, 110, D24307, doi:10.1029/2005JD005973, 2005. 2391
- Motte, E., Ricaud, P., Gabard, B., Niclas, M., and Gangneron, F.: A 22-GHz Mobile Microwave Radiometer (MobRa) for the study of middle atmospheric water vapor, *IEEE T. Geosci. Re-*

MIAWARA-C

C. Straub et al.

[Title Page](#)[Abstract](#)[Introduction](#)[Conclusions](#)[References](#)[Tables](#)[Figures](#)[⏪](#)[⏩](#)[◀](#)[▶](#)[Back](#)[Close](#)[Full Screen / Esc](#)[Printer-friendly Version](#)[Interactive Discussion](#)

mote, 46, 3104–3114, 2008. 2392

Müller, S., Murk, A., Monstein, C., Kämpfer, N., and Meyer, H.: Microwave remote sensing of stratospheric trace gases using digital Fast Fourier Transform spectrometers, in: GeMiC 2006 – Conference Proceedings, 2006. 2397

5 Murtagh, D., Frisk, U., Merino, F., Ridal, M., Jonsson, A., Stegman, J., Witt, G., Eriksson, P., Jiménez, C., Megie, G., de la Noë, J., Ricaud, P., Baron, P., Pardo, J. R., Hauchcorne, A., Llewellyn, E. J., Degenstein, D. A., Gattinger, R. L., Lloyd, N. D., Evans, W. F., McDade, I. C., Haley, C. S., Sioris, C., von Savigny, C., Solheim, B. H., McConnell, J. C., Strong, K., Richardson, E. H., Leppelmeier, G. W., Kyrölä, E., Auvinen, H., and Oikarinen, L.: An overview of the Odin atmospheric mission, *Can. J. Phys.*, 80, 309–319, 2002. 2391

10 Nedoluha, G. E., Bevilacqua, R. M., Gomez, R. M., Thacker, D. L., Waltman, W. B., and Pauls, T. A.: Ground-based measurements of water vapor in the middle atmosphere, *J. Geophys. Res.*, 100, 2927–2937, 1995. 2392

15 Nedoluha, G. E., Gomez, R. M., Hicks, B. C., Bevilacqua, R. M., Russell, J., Connor, B. J., and Lambert, A.: A comparison of middle atmospheric water vapor as measured by WVMS, EOS-MLS, and HALOE, *J. Geophys. Res.*, 112, D24S39, doi:10.1029/2007JD008757, 2007. 2392

Parrish, A., Dezafrá, R. L., Solomon, P. M., and Barrett, J. W.: A ground-based technique for millimeter wave spectroscopic observations of stratospheric trace constituents, *Radio Sci.*, 23, 106–118, 1988. 2396

20 Plumb, R. A.: A “tropical pipe” model of stratospheric transport, *J. Geophys. Res.*, 101, 3957–3972, 1996. 2391

Poynter, R. L. and Pickett, M.: Submillimeter, millimeter, and microwave spectral line catalog, *Appl. Optics*, 24, 2235–2240, 1985. 2409

25 Rodgers, C. D.: *Inverse Methodes for Atmospheric Soundings*, World Scientific Publishing Co. Pte. Ltd, Singapore, 2000. 2393, 2409

Straub, C.: Development of a 22 GHz correlating Radiometer for the observation of Stratospheric Water Vapor, Master’s thesis, University of Bern, 2008. 2398

30 Straub, C., Murk, A., Teniente, J., and Kämpfer, N.: Optical design for a compact 22 GHz radiometer for middle atmospheric water vapor, in: EUCAP 2007 Conference proceedings, 2007. 2394

Teniente, J., Gonzalo, R., and del Rio, C.: Choked gaussian antenna: extremely low sidelobe compact antenna design, *IEEE Antenn. Wirel. Pr.*, 1, 200–202, 2002. 2395

Thacker, D. L., Bevilacqua, R. M., Waltman, W. B., Pauls, T. A., Gomez, R. M., Nedoluha, G. E., and Schwartz, R. R.: Ground-based sensing of water vapor in the stratosphere and mesosphere, *IEEE T. Instrum. Meas.*, 44, 355–359, 1995. 2392

5 Waters, J., Froidevaux, L., Harwood, R., Jarno, R., Pickett, H., Read, W., Siegel, P., Cofield, R., Filipiak, M., Flower, D., Holden, J., Lau, G., Livesey, N., Manney, G., Pumphrey, H., Santee, M., Wu, D., Cuddy, D., Lay, R., Loo, M., Perun, V., Schwartz, M., Stek, P., Thurstans, R., Boyles, M., Chandra, S., Chavez, M., Chen, G.-S., Chudasama, B., Dodge, R., Fuller, R., Girard, M., Jiang, J., Jiang, Y., Knosp, B., LaBelle, R., Lam, J., Lee, K., Miller, D., Oswald, J., Patel, N., Pukala, D., Quintero, O., Scaff, D., Snyder, W., Tope, M., Wagner, P., and Walch, M.:
10 The Earth Observing System Microwave Limb Sounder (EOS MLS) on the Aura satellite, *IEEE T. Geosci. Remote*, 44, 1075–1092, 2006. 2391

AMTD

3, 2389–2432, 2010

MIAWARA-C

C. Straub et al.

Title Page

Abstract

Introduction

Conclusions

References

Tables

Figures

⏪

⏩

◀

▶

Back

Close

Full Screen / Esc

Printer-friendly Version

Interactive Discussion



MIAWARA-C

C. Straub et al.

[Title Page](#)[Abstract](#)[Introduction](#)[Conclusions](#)[References](#)[Tables](#)[Figures](#)[⏪](#)[⏩](#)[◀](#)[▶](#)[Back](#)[Close](#)[Full Screen / Esc](#)[Printer-friendly Version](#)[Interactive Discussion](#)**Table 1.** Key parameters and specifications of MIAWARA-C

Optical system	choked gaussian horn combined with parabolic mirror, HPBW 5.0°
Receiver type	correlation receiver with digital cross correlation FFT spectrometer
Receiver operation mode	Single side band
RF-frequency range	22.012–22.411 GHz
Frequency resolution	30.5 kHz
Calibration	Balancing
Absolute calibration	hot, cold

MIAWARA-C

C. Straub et al.

Title Page

Abstract

Introduction

Conclusions

References

Tables

Figures

◀

▶

◀

▶

Back

Close

Full Screen / Esc

Printer-friendly Version

Interactive Discussion



Table 2. Pointing of MIAWARA-C in elevation and azimuth direction determined with the sky- and the sun scanning method.

	Sky Scanning 30 Jul 2009	Sun Scanning 5 Aug 2009
pointing in azimuth [°]	N/A	0.948
pointing offset in elevation [°]	-0.012	-0.004

[Title Page](#)[Abstract](#)[Introduction](#)[Conclusions](#)[References](#)[Tables](#)[Figures](#)[◀](#)[▶](#)[◀](#)[▶](#)[Back](#)[Close](#)[Full Screen / Esc](#)[Printer-friendly Version](#)[Interactive Discussion](#)**Table 3.** Estimates of the errors of the relevant forward model parameters

Parameter	Estimated error
Measurement noise	depends on integration time here 0.011 K
Temperature profile	5 K
Calibration	7% of factor for the tropospheric correction
Line intensity S	$8.7 \times 10^{-22} \text{ m}^2 \text{ Hz}$
Air broadening γ_{air}	1014 Hz/Pa

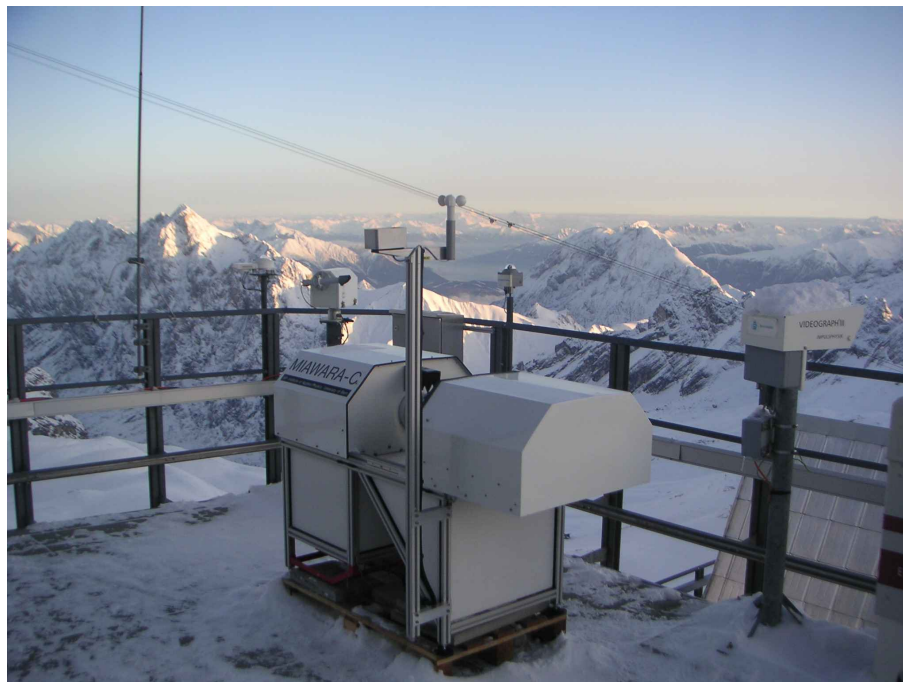


Fig. 1. MIAWARA-C during the ARIS-Campaign on the Zugspitze.

AMTD

3, 2389–2432, 2010

MIAWARA-C

C. Straub et al.

Title Page

Abstract

Introduction

Conclusions

References

Tables

Figures

◀

▶

◀

▶

Back

Close

Full Screen / Esc

Printer-friendly Version

Interactive Discussion



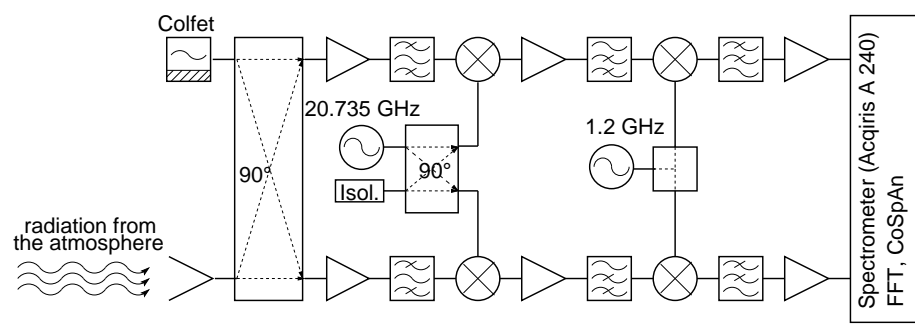


Fig. 2. Block diagram of the correlation receiver of MIAWARA-C.

Title Page

Abstract Introduction

Conclusions References

Tables Figures

⏪ ⏩

◀ ▶

Back Close

Full Screen / Esc

Printer-friendly Version

Interactive Discussion



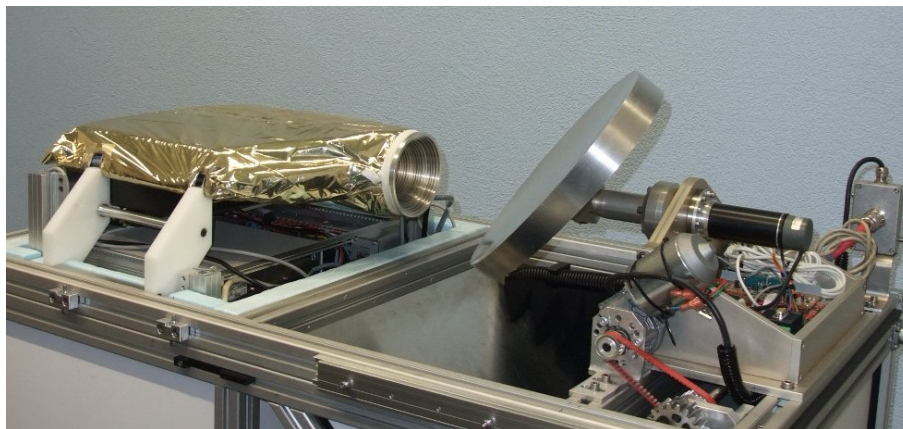


Fig. 3. Optical system of MIAWARA-C.

MIAWARA-C

C. Straub et al.

Title Page

Abstract

Introduction

Conclusions

References

Tables

Figures

◀

▶

◀

▶

Back

Close

Full Screen / Esc

Printer-friendly Version

Interactive Discussion



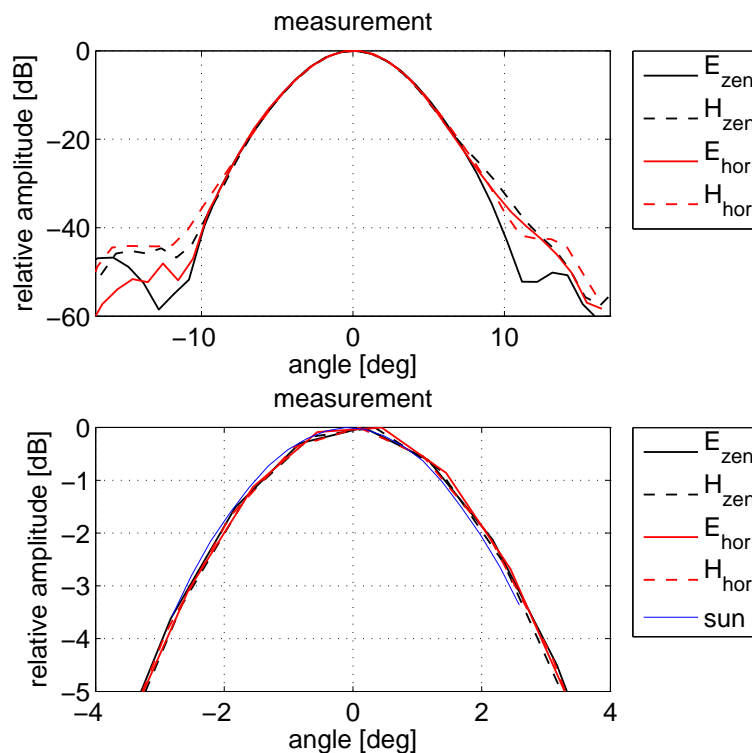


Fig. 4. Farfield at 22.235 GHz of the optical system of MIAWARA-C measured with two different methods. Laboratory measurements deliver (E- and H-plane) in horizontal (red) and zenith (black) direction while the measurements using the sun as a transmitter result in a general pattern (blue).

[Title Page](#)[Abstract](#)[Introduction](#)[Conclusions](#)[References](#)[Tables](#)[Figures](#)[◀](#)[▶](#)[◀](#)[▶](#)[Back](#)[Close](#)[Full Screen / Esc](#)[Printer-friendly Version](#)[Interactive Discussion](#)

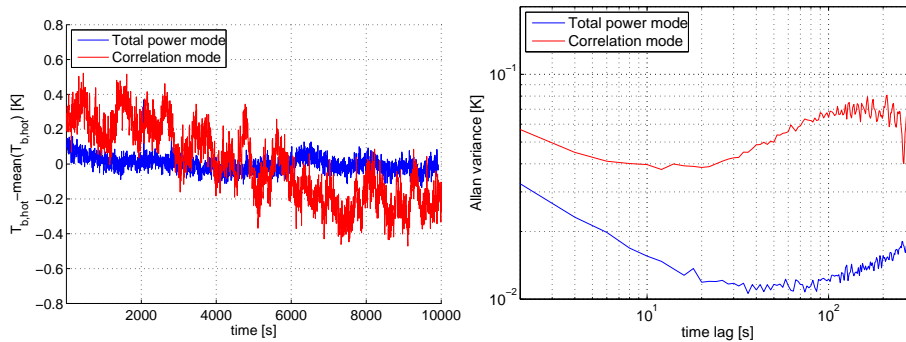


Fig. 5. Stability of the receiver of MIAWARA-C in the correlation- and the total power mode. Timeseries of the deviation of the calibrated data from the mean value (left) and Allan variance (right), $\tau=2$ s and $\Delta\nu=30$ kHz.

Title Page

Abstract

Introduction

Conclusions

References

Tables

Figures

◀

▶

◀

▶

Back

Close

Full Screen / Esc

Printer-friendly Version

Interactive Discussion



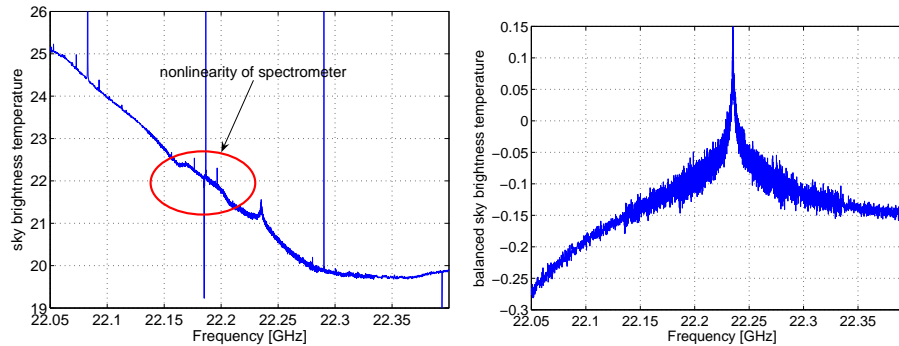


Fig. 6. Spectrum of MIAWARA-C after one day of integration calibrated with the method in Eq. (4) (left) and with the balancing calibration in Eq. (5) (right).

[Title Page](#)[Abstract](#)[Introduction](#)[Conclusions](#)[References](#)[Tables](#)[Figures](#)[⏪](#)[⏩](#)[◀](#)[▶](#)[Back](#)[Close](#)[Full Screen / Esc](#)[Printer-friendly Version](#)[Interactive Discussion](#)

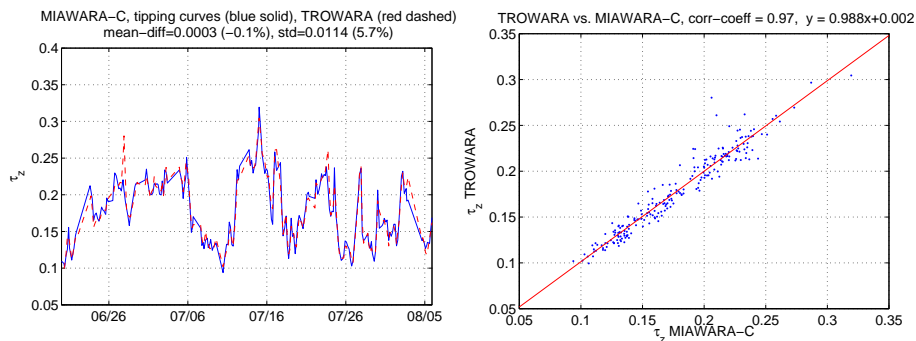


Fig. 7. Left panel: time series of 4 h means of τ_z derived from MIAWARA-C tipping curves (mean value of 22.235 ± 0.1 GHz) and TROWARA measurements at a constant elevation angle of 40° (mean value of 22.235 ± 0.2 GHz). Right panel: correlation between the data obtained in the time period from 20 June to 5 August 2009.

[Title Page](#)
[Abstract](#)
[Introduction](#)
[Conclusions](#)
[References](#)
[Tables](#)
[Figures](#)
[⏪](#)
[⏩](#)
[◀](#)
[▶](#)
[Back](#)
[Close](#)
[Full Screen / Esc](#)
[Printer-friendly Version](#)
[Interactive Discussion](#)

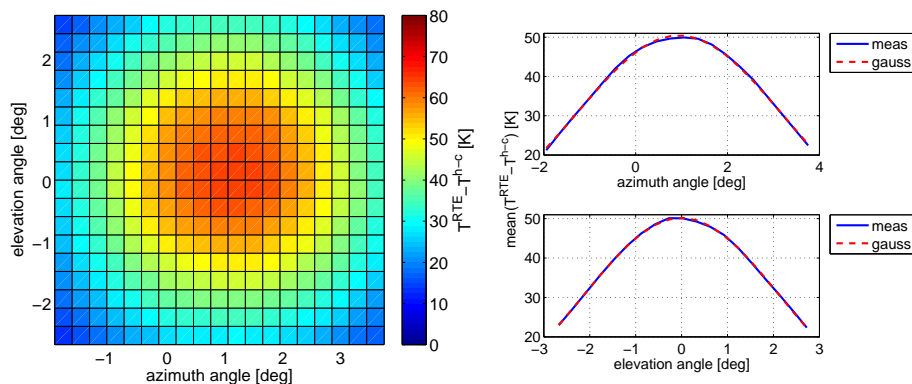



Fig. 8. Calibration of the elevation and azimuth pointing of MIAWARA-C using the sun scanning method. Left panel: result of sun scanning interpolated to rectangular coordinate system relative to the sun. Right panel: Gaussian curve fitted to weighted mean value of the antenna pattern in azimuth and elevation direction.

[Title Page](#)[Abstract](#)[Introduction](#)[Conclusions](#)[References](#)[Tables](#)[Figures](#)[◀](#)[▶](#)[◀](#)[▶](#)[Back](#)[Close](#)[Full Screen / Esc](#)[Printer-friendly Version](#)[Interactive Discussion](#)

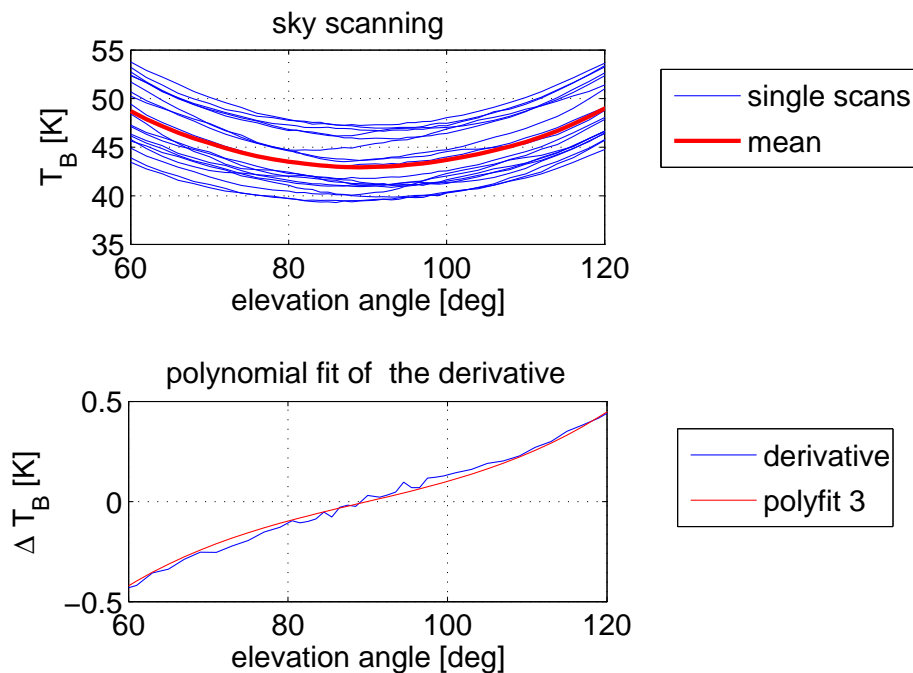


Fig. 9. Calibration of the elevation pointing of MIAWARA-C using the sky scanning method. Upper panel: calibrated sky scans. Lower panel: first derivative of sky brightness temperature and polynomial fit of third degree.

[Title Page](#)[Abstract](#)[Introduction](#)[Conclusions](#)[References](#)[Tables](#)[Figures](#)[◀](#)[▶](#)[◀](#)[▶](#)[Back](#)[Close](#)[Full Screen / Esc](#)[Printer-friendly Version](#)[Interactive Discussion](#)

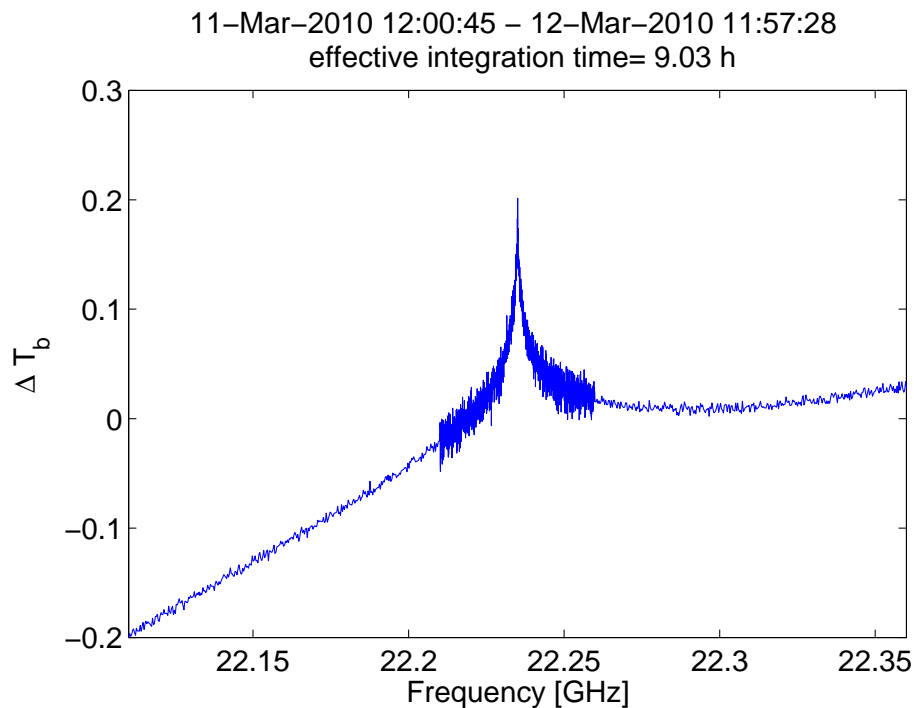


Fig. 10. Typical one day spectrum of MIAWARA-C measured during the Lapbiat campaign. The difference in the noise levels in different frequency ranges is due to a frequency binning of 10 channels used on the wings of the spectrum for data reduction.

[Title Page](#)[Abstract](#)[Introduction](#)[Conclusions](#)[References](#)[Tables](#)[Figures](#)[◀](#)[▶](#)[◀](#)[▶](#)[Back](#)[Close](#)[Full Screen / Esc](#)[Printer-friendly Version](#)[Interactive Discussion](#)

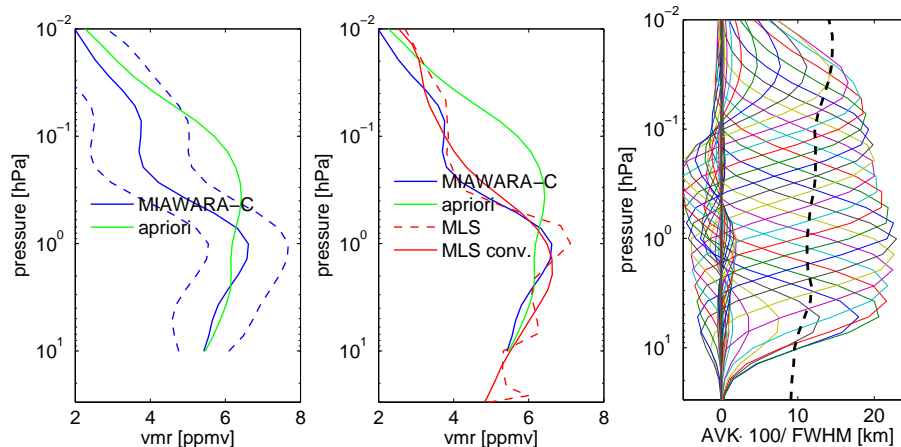


Fig. 11. Water vapor profile retrieved from the one day spectrum shown in Fig. 10 plotted together with the apriori profile and the upper limit for the systematic plus random $2\text{-}\sigma$ and compared to the profile of a close MLS overpass (67.5° N , 21.0° E) in the middle plot. The averaging kernels of MIAWARA-C are shown on the right together with the FWHM of each of the kernels.

[Title Page](#)
[Abstract](#)
[Introduction](#)
[Conclusions](#)
[References](#)
[Tables](#)
[Figures](#)
[◀](#)
[▶](#)
[◀](#)
[▶](#)
[Back](#)
[Close](#)
[Full Screen / Esc](#)
[Printer-friendly Version](#)
[Interactive Discussion](#)

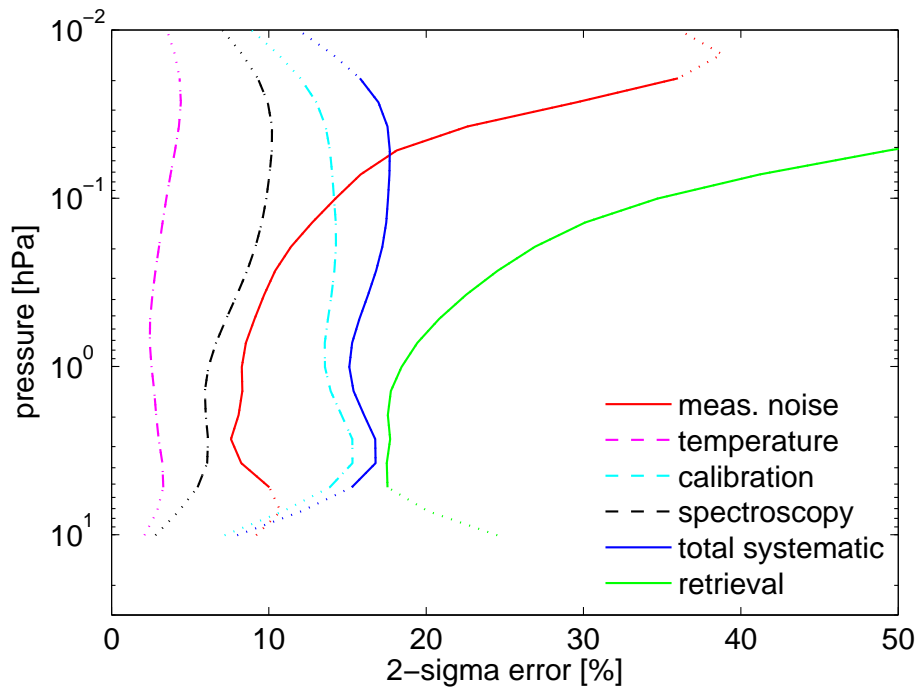



Fig. 12. Estimated $2\text{-}\sigma$ errors in the retrieved profile resulting from different families of uncertainty.

Title Page

Abstract

Introduction

Conclusions

References

Tables

Figures

◀

▶

◀

▶

Back

Close

Full Screen / Esc

Printer-friendly Version

Interactive Discussion



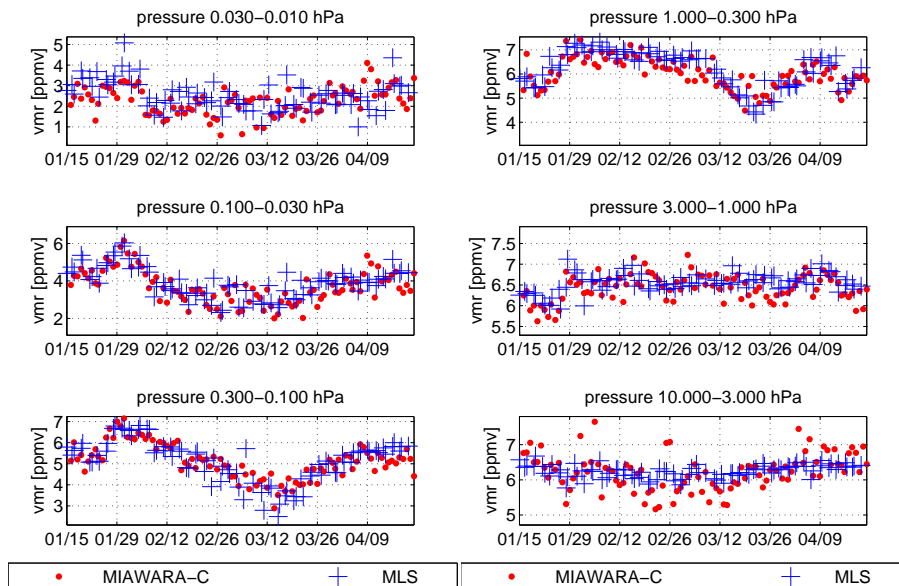


Fig. 13. Timeseries of middle atmospheric H_2O for 6 pressure ranges between 10 and 0.03 hPa as observed by MIAWARA-C and MLS during the Laplat campaign. A mean value of the H_2O -vmr within the pressure ranges indicated is used to account for the different altitude resolutions of the two instruments.

[Title Page](#)
[Abstract](#)
[Introduction](#)
[Conclusions](#)
[References](#)
[Tables](#)
[Figures](#)
[◀](#)
[▶](#)
[◀](#)
[▶](#)
[Back](#)
[Close](#)
[Full Screen / Esc](#)
[Printer-friendly Version](#)
[Interactive Discussion](#)

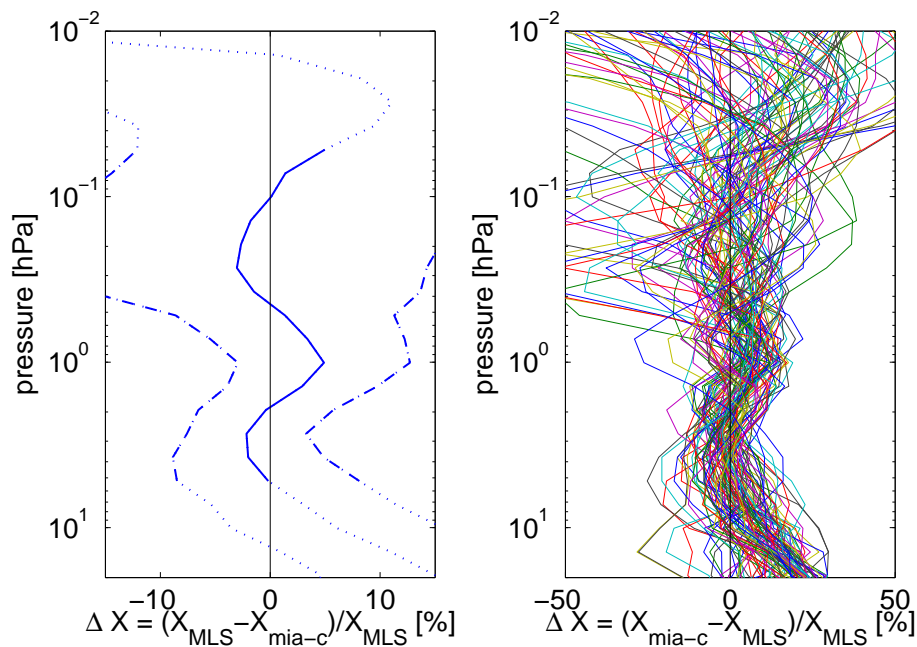



Fig. 14. Relative difference between the measurements of MIAWARA-C and MLS, mean value and standard deviation left and single profile comparisons right.

[Title Page](#)
[Abstract](#)
[Introduction](#)
[Conclusions](#)
[References](#)
[Tables](#)
[Figures](#)
[◀](#)
[▶](#)
[◀](#)
[▶](#)
[Back](#)
[Close](#)
[Full Screen / Esc](#)
[Printer-friendly Version](#)
[Interactive Discussion](#)
